

# Temperature anisotropy instabilities driven by intermittent velocity shears in the solar wind

Simon Opie<sup>1†</sup>, Daniel Verscharen<sup>1</sup> Christopher H. K. Chen<sup>2</sup>  
 Christopher J. Owen<sup>1</sup> Philip A. Isenberg<sup>3</sup> Luca Sorriso-Valvo<sup>4,5</sup> Luca  
 Franci<sup>6</sup> Lorenzo Matteini<sup>7</sup>

<sup>1</sup>Mullard Space Science Laboratory, University College London, Dorking, RH5 6NT, UK

<sup>2</sup>Department of Physics and Astronomy, Queen Mary University of London, London, E1 4NS, UK

<sup>3</sup>Space Science Center, University of New Hampshire, Durham, NH 03824, USA

<sup>4</sup>CNR, Istituto per la Scienza e la Tecnologia dei Plasmi, via Amendola 122/D, 70126 Bari, Italy

<sup>5</sup>Space and Plasma Physics, School of Electrical Engineering and Computer Science, KTH Royal Institute of Technology, Teknikringen 31, 11428 Stockholm, Sweden

<sup>6</sup>Department of Mathematics, Physics and Electrical Engineering, Northumbria University, Newcastle upon Tyne, NE1 8ST, UK

<sup>7</sup>The Blackett Laboratory, Department of Physics, Imperial College London, London, SW7 2AZ, UK

(Received xx; revised xx; accepted xx)

Where and under what conditions the transfer of energy between electromagnetic fields and particles takes place in the solar wind remains an open question. We investigate the conditions that promote the growth of kinetic instabilities predicted by linear theory, to infer how turbulence and temperature-anisotropy-driven instabilities are interrelated. Using a large dataset from Solar Orbiter, we introduce the radial rate of strain, a novel measure computed from single-spacecraft data, that we interpret as a proxy for the double-adiabatic strain rate. The solar wind exhibits high absolute values of the radial rate of strain at locations with large temperature anisotropy. We measure the kurtosis and skewness of the radial rate of strain from the statistical moments to show that it is non-Gaussian for unstable intervals and increasingly intermittent at smaller scales with a power-law scaling. We conclude that the velocity field fluctuations in the solar wind contribute to the presence of temperature anisotropy sufficient to create potentially unstable conditions.

## 1. Introduction

The solar wind is a weakly collisional, magnetised plasma characterised by kinetic processes that influence its dynamic evolution in ways that are not fully understood. The expansion of the solar wind into interplanetary space in the presence of a decreasing background magnetic field (Matteini *et al.* 2007, 2012) implies that the particle distributions should be highly anisotropic by the time the plasma reaches a distance of  $\sim 1$  au from the Sun (Verscharen *et al.* 2016). The double-adiabatic (CGL; Chew *et al.* 1956) expansion of the solar wind predicts a decline in  $T_{\perp}/T_{\parallel}$  with distance from the Sun, where  $T_{\perp}$  ( $T_{\parallel}$ ) is the proton temperature perpendicular (parallel) to the magnetic field direction (Matteini *et al.* 2007; Cranmer *et al.* 2009). However, observations at 1 au show that the solar wind

† Email address for correspondence: simon.opie.18@ucl.ac.uk

is on average almost isotropic with respect to the background magnetic field, albeit with significant variability in temperature anisotropy about the isotropic equilibrium (Marsch *et al.* 1982; Kasper *et al.* 2002; Bale *et al.* 2009; Maruca *et al.* 2011; Isenberg *et al.* 2013; Coburn *et al.* 2022).

The presence of temperature anisotropy in the solar wind is also linked to turbulence. Solar-wind turbulence facilitates a non-linear transfer of energy from larger to smaller scales via a Kolmogorov-like inertial range, leading to the dissipation of energy at kinetic scales (Kolmogorov 1941; Alexandrova *et al.* 2013; Bruno & Carbone 2013; Kiyani *et al.* 2015; Chen 2016; Marino & Sorriso-Valvo 2023). This non-linear energy transfer occurs via a cascade which is inherently anisotropic in the distribution of its spectral power with respect to the wavevector of the fluctuations, with  $k_{\perp} \gg k_{\parallel}$ , where  $k_{\perp}$  ( $k_{\parallel}$ ) is the component of the wavevector perpendicular (parallel) to the magnetic field direction (Cho & Vishniac 2000; Schekochihin *et al.* 2009; Wicks *et al.* 2011; Horbury *et al.* 2012; Oughton *et al.* 2015; Chen *et al.* 2016; Schekochihin 2022). Some solar wind models predict that the turbulent cascade is responsible for the temperature-anisotropic heating of the plasma (Parashar *et al.* 2009; Chandran *et al.* 2010; Howes 2015). Considering the expectations based on CGL expansion and temperature-anisotropic heating models, the observation of approximately isotropic plasma conditions on average suggests that additional processes act to restore isotropy through the transfer of energy (Marsch *et al.* 1982). The stability of the solar wind depends on the simultaneous contributions of all species in the plasma to its free energy (Chen *et al.* 2016) but here we consider only the protons.

A class of kinetic instabilities is triggered when the proton temperature anisotropy exceeds certain thresholds for the production of plasma waves and non-propagating modes. These instabilities transfer energy from the particles to electromagnetic fields and this transfer restores the proton distribution towards a stable state closer to isotropy (Gary 1976, 1993; Hellinger *et al.* 2006). At large scales, compressive fluctuations can drive temperature anisotropy leading to wave-driven instabilities that eventually reduce anisotropy through pitch-angle scattering of protons (Verscharen *et al.* 2016), while at small scales kinetic instabilities predicted by linear theory, redistribute energy through wave-particle interaction (Gary 1993; Kasper *et al.* 2002; Hellinger *et al.* 2011, 2013; Howes 2015).

Proton-kinetic processes, such as temperature-anisotropy-driven instabilities, predominantly occur on scales near the small-scale end of the inertial range (Gary 2015). Contrary to the framework of traditional linear theory, kinetic instabilities in the solar wind operate in inhomogeneous and non-constant conditions due to the ubiquitous solar-wind turbulence (Coleman 1968; Frisch *et al.* 1978; Tu & Marsch 1995; Chen 2016; Verscharen *et al.* 2019; Opie *et al.* 2022, 2023). In developing a more robust understanding of where and under what conditions energy transfer takes place, it is therefore important to fully capture the interplay between kinetic and turbulent features at the appropriate scales in the solar wind (Osman *et al.* 2012; Chen 2016; Sorriso-Valvo *et al.* 2018a; Opie *et al.* 2022, 2023; Arzamasskiy *et al.* 2023).

The solar-wind turbulence is intermittent and consistent with the model of multifractality (Frisch & Kolmogorov 1995), meaning that the fluctuations at different scales are not equally space filling and instead contain coherent structures such as current sheets and velocity shear layers (Sorriso-Valvo *et al.* 1999; Greco *et al.* 2008; Osman *et al.* 2013; Servidio *et al.* 2014; Matthaeus *et al.* 2015; Qudsi *et al.* 2020). These structures extend across scales in the inertial range and exhibit a statistical scaling relationship that indicates that they are self-affine (Carbone *et al.* 1995, 1996; Sorriso-Valvo *et al.* 1999; Kiyani *et al.* 2006; Hnat *et al.* 2007).

---

Interval	Heliocentric Distance ( $R_S$ )	Number of Datapoints
2020 October 07-18	205	185 923
2021 April 22-28	190	131 481
2021 May 05-11	180	131 849
2021 June 10-13	200	79 641
2021 July 06-11	190	117 427
2021 July 20-24	180	88 429
2021 October 09-12	150	81 362
2021 October 19-26	160	159 404
2021 November 02-07	175	132 750
2021 November 09-14	180	86 201
2021 November 16-19	190	85 833
2021 December 28 - 2022 January 02	215	128 048
2022 January 04-08	215	58 773

---

TABLE 1. Data selection from the Solar Orbiter Archive with approximate heliocentric distance (in solar radii,  $R_S$ ) for each data interval

We hypothesise that the turbulent and intermittent velocity field in the solar wind is dynamically important for driving the temperature anisotropy of the plasma protons. Using a large observational dataset, we localise conditions in the solar wind at and beyond the thresholds for the proton-driven oblique firehose instability when  $T_{\perp}/T_{\parallel} < 1$  (Hellinger & Trávníček 2008; Markovskii & Vasquez 2022) and mirror-mode instability when  $T_{\perp}/T_{\parallel} > 1$  (Kunz *et al.* 2014; Hellinger *et al.* 2017), which place effective boundaries for temperature anisotropy in the solar wind (Hellinger *et al.* 2006; Bale *et al.* 2009; Gary 2015). Working directly from the dynamical equations, we develop and analyse a quantitative measure for the impact of velocity shears on the temperature anisotropy, the radial rate of strain. We measure the third and fourth statistical moments of the radial rate of strain, the velocity field, and the magnetic field, from which we infer where, in terms of turbulent structures in the solar wind, these instabilities are located.

We set out details of our data analysis in Section 2. In Section 3, we develop and evaluate our novel measure of the radial rate of strain, a one-dimensional proxy for the three-dimensional double-adiabatic strain rate. In Section 4, we calculate the skewness and kurtosis of the radial rate of strain, the magnetic field and the velocity field. We discuss the significance of our results in Section 5 and conclude with recommendations for further work in Section 6.

## 2. Data Analysis

### 2.1. Dataset

Our dataset, which is a significant extension of that used by Opie *et al.* (2022), comprises  $\approx 1.5$ M datapoints, as detailed in Table 1. Our data are taken from the Solar Orbiter public archive<sup>†</sup>. We use data from two of the in-situ instruments on board the spacecraft which make measurements of the solar wind; namely the magnetic-field vector from the Magnetometer (MAG) at 8 Hz cadence (Horbury 2020) and the proton moments from the Proton Alpha Sensor (PAS). For the periods discussed here, PAS takes a 1 s sample every 4 s. PAS is part of the Solar Wind Analyser (SWA) instrument suite (Owen 2020). For this study, we work in the  $(R, T, N)$  coordinate system, where the axis  $R$

<sup>†</sup> <http://soar.esac.esa.int/soar/>

points radially outwards from the Sun,  $T$  is given by the cross-product between the Sun's rotation vector and  $R$ , and  $N$  completes the right-handed triad.

The relative error for the PAS data is  $\approx 0.27\%$  for the velocity measurements (Louarn 2021). For our dataset, this represents an average absolute error of  $\approx 1.2 \text{ km s}^{-1}$ .

Since we employ two-point field increments in this analysis, we use continuous data intervals of 4–7 days duration, subject to data availability. We exclude PAS datapoints for which the solar wind bulk velocity  $< 325 \text{ km s}^{-1}$  or when measurements are outside the recommended PAS quality factor  $\leq 0.2$ . No attempt is made to eliminate any structures, such as shocks or interplanetary coronal mass ejections (ICMEs), from the dataset. Reference to the Helio4Cast catalogue† for ICMEs observed by Solar Orbiter gives three ICMEs in total within our combined dataset. These occurred on 2021 May 06, 2021 May 10, and 2021 November 03 for an aggregated duration of 79.16 hours of our total observational timeframe of 80 days (Möstl 2017; Möstl *et al.* 2020).

Solar Orbiter has provided a continuous high-resolution dataset of the pristine solar wind for both magnetic and proton velocity field analysis (Louarn 2021; Zouganelis *et al.* 2022). This enables our two-point field increment method to be statistically robust on timescales that equivalent to the scales needed to observe unstable intervals (Opie *et al.* 2022).

## 2.2. Data processing

We rotate the proton pressure tensor to align with the local associated magnetic field and create a timeseries for  $\beta_{\parallel} \equiv 8\pi n_p k_B T_{\parallel} / B^2$ , where  $n_p$  is the proton number density,  $k_B$  is the Boltzmann constant, and  $B$  is the magnetic field strength averaged over the associated 1 s PAS measurement interval. From the proton pressure tensor, we then calculate the ratio  $T_{\perp} / T_{\parallel}$  for each PAS measurement.

In order to identify intervals in our dataset for which linear theory predicts the growth of kinetic instabilities, we require thresholds for the growth of the specific anisotropy-driven kinetic instabilities of interest. We base our identification of unstable intervals on the parametric approximation for the instability thresholds in the form

$$\frac{T_{\perp}}{T_{\parallel}} = 1 + \frac{a}{(\beta_{\parallel} - c)^b}, \quad (2.1)$$

where  $a$ ,  $b$ , and  $c$  are constants with values given for each instability for a range of instability maximum growth rates by Verscharen *et al.* (2016). We use the constants given for a maximum growth rate of  $\gamma_m = 10^{-2} \Omega_p$ , where  $\Omega_p$  is the proton gyrofrequency. We evaluate these instability thresholds for the oblique firehose (OF) and for the mirror-mode (M) instabilities. For reference, we also include the instability threshold for the Alfvén/ion-cyclotron (A/IC) instability in part of our analysis.

We analyse data distributed in anisotropy - plasma beta ( $T_{\perp} / T_{\parallel} - \beta_{\parallel}$ ) parameter space that is bounded by these thresholds. We define the unstable intervals as comprising those data points that lie above the thresholds, while we characterise all data below the thresholds as stable. Consequently, the plasma is considered unstable against M and A/IC instabilities if  $T_{\perp} / T_{\parallel}$  is greater than the value given by the right-hand side of Eq. (2.1), while it is considered unstable against the OF instability if  $T_{\perp} / T_{\parallel}$  is less than the value given by the right-hand side of Eq. (2.1), with in each case the constants chosen for the respective instability.

† [https://helioforecast.space/static/sync/icmecat/HELIO4CAST\\_ICMECAT\\_v22.csv](https://helioforecast.space/static/sync/icmecat/HELIO4CAST_ICMECAT_v22.csv)

### 3. Radial strain

In this section, we use a single-species (proton) fluid model of space plasma that derives anisotropy directly from the effect of fluid strain on the pressure tensor. We define the radial rate of strain  $\Gamma_R$  as a proxy for the strain rate in fully three-dimensional turbulence for this analysis, which we believe to be a novel technique. We then use this measure to test our hypothesis that intermittent velocity shear is dynamically important for the generation of the observed temperature anisotropy in the solar wind.

#### 3.1. Method: Determination of the radial strain

We examine the evolution of pressure anisotropy based on the first three moments of the proton distribution function under CGL analysis (Chew *et al.* 1956; Kulsrud 1984). We take the form of the equation for pressure anisotropy given by Squire *et al.* (2023) which assumes that the pressure tensor is invariant to rotation about the magnetic field direction:

$$\begin{aligned} \frac{d}{dt}(p_{\perp} - p_{\parallel}) = & (p_{\perp} + 2p_{\parallel})\hat{\mathbf{b}}\hat{\mathbf{b}} : \nabla\mathbf{v} - (2p_{\perp} - p_{\parallel})\nabla \cdot \mathbf{v} \\ & - \nabla \cdot [(q_{\perp} - q_{\parallel})\hat{\mathbf{b}}] - 3q_{\perp}\nabla \cdot \hat{\mathbf{b}} - \nu_c(p_{\perp} - p_{\parallel}), \end{aligned} \quad (3.1)$$

where  $p_{\perp}$  and  $p_{\parallel}$  are the proton pressure tensor components perpendicular and parallel to the magnetic field,  $\hat{\mathbf{b}} = \mathbf{B}/B$ ,  $\mathbf{v}$  is the proton bulk velocity,  $q_{\perp}$  and  $q_{\parallel}$  are the proton heat fluxes perpendicular and parallel to the magnetic field direction, and  $\nu_c$  is the proton collisional relaxation frequency for temperature anisotropy. The first two terms on the right-hand side of Equation (3.1) describe how plasma bulk flows directly affect pressure anisotropy through shear and compression. We assume that  $\nu_c = 0$  and  $q_{\perp} = q_{\parallel} = 0$  following the arguments of Del Sarto & Pegoraro (2018).

These assumptions allow us to formulate a new proxy measure for the driving of pressure anisotropy by plasma motion based on plasma measurements sampled along the radial direction by a single spacecraft. We use Taylor's hypothesis (Taylor 1938) to transpose spatial partial derivatives to temporal partial derivatives and employ increments to replace  $\nabla \cdot \mathbf{v}$  and  $\nabla\mathbf{v}$ . After these transformations, we define the radial rate of strain as

$$\Gamma_R = \frac{1}{\tau} \left[ \left[ (p_{\perp} + 2p_{\parallel}) \left( \hat{b}_R \hat{b}_R \Delta v_R + \hat{b}_T \hat{b}_R \Delta v_T + \hat{b}_N \hat{b}_R \Delta v_N \right) \right] - (2p_{\perp} - p_{\parallel}) \Delta v_R \right], \quad (3.2)$$

where  $\tau$  is the time increment between measurement points (i.e., the measurement cadence) and  $\Delta\phi$  denotes the scale-dependent increment  $\Delta\phi = \phi(t) - \phi(t + \tau)$  of any time-dependent observable  $\phi$  in the spacecraft reference frame.

Following the interpretation of the first and second terms in Equation (3.1), we decompose Equation (3.2) into proxies for the incompressible ( $\Gamma_{RI}$ ) and compressible ( $\Gamma_{RC}$ ) contributions to  $\Gamma_R$  as

$$\Gamma_{RI} = \frac{1}{\tau} \left[ (p_{\perp} + 2p_{\parallel}) \left( \hat{b}_R \hat{b}_R \Delta v_R + \hat{b}_T \hat{b}_R \Delta v_T + \hat{b}_N \hat{b}_R \Delta v_N \right) \right] \quad (3.3)$$

and

$$\Gamma_{RC} = \frac{1}{\tau} \left[ (p_{\parallel} - 2p_{\perp}) \Delta v_R \right]. \quad (3.4)$$

We set  $\tau = 8$  s, which results in an average relative value of  $\Delta v_j/|\mathbf{v}|$  for our intervals of 0.48%. We check that all data with small  $\Delta v_j$  values make a negligible contribution to  $\Gamma_R$  and so the relevant datapoints are well above the PAS relative error. Any systematic errors due to bias offsets in any quantity  $\phi$  are eliminated through the process of

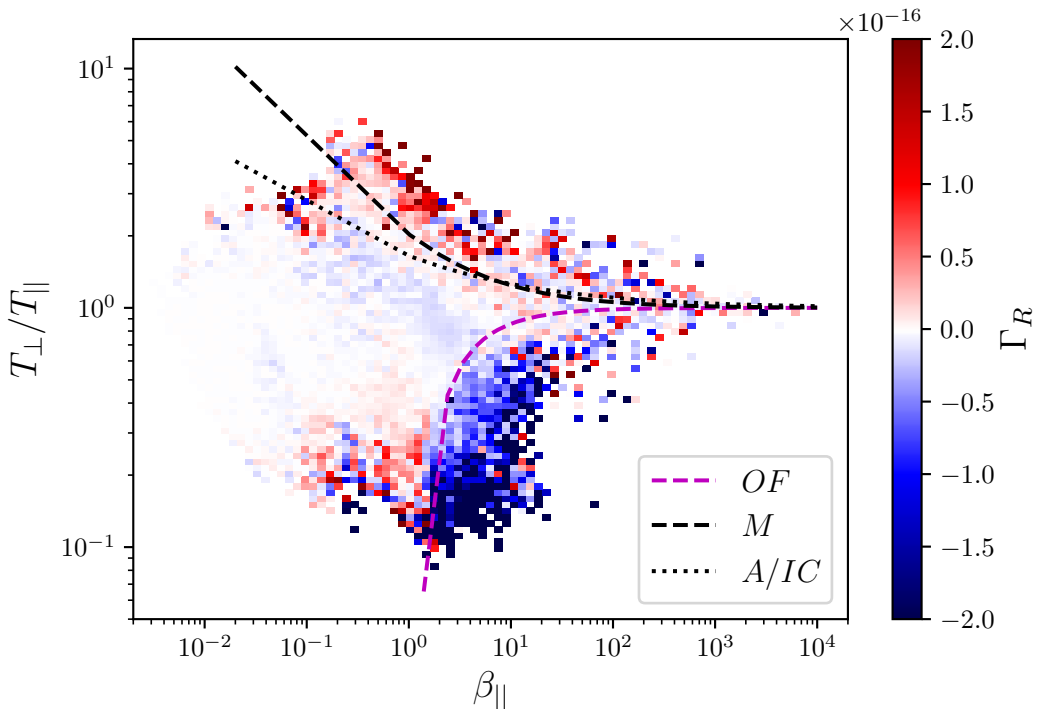


FIGURE 1. Distribution of  $\Gamma_R$  as bin averages in  $T_{\perp}/T_{\parallel}-\beta_{\parallel}$  parameter space. We overplot the instability thresholds for the Oblique Firehose (OF), Alfvén/Ion cyclotron (A/IC), and Mirror-mode (M) instabilities.

calculating the difference  $\Delta\phi$ . We exclude any data points for which an increment of  $\tau = 8$  s cannot be calculated due to data gaps.

### 3.2. Results: The radial strain of stable and unstable plasma intervals

We calculate  $\Gamma_R$  from Equation (3.2) for each datapoint in our dataset after the elimination of data gaps and plot the bin-averaged values in a two-dimensional histogram in  $T_{\perp}/T_{\parallel}-\beta_{\parallel}$  parameter space in Figure 1. We also calculate  $\Gamma_{RI}$  from Equation (3.3) and  $\Gamma_{RC}$  from Equation (3.4) and plot these separately in two-dimensional histograms in  $T_{\perp}/T_{\parallel}-\beta_{\parallel}$  parameter space in Figures 2 and 3, respectively.

According to Figure 1, the unstable intervals show on average high absolute values, relative to the stable data, of  $\Gamma_R$ , with  $\Gamma_R > 0$  in the parameter space associated with the M and A/IC instabilities and  $\Gamma_R < 0$  in the parameter space associated with the OF instability. This relation is equally maintained for both  $\Gamma_{RI}$  and  $\Gamma_{RC}$  as shown in Figures 2 and 3, although the signal varies with  $\beta_{\parallel}$  and  $T_{\perp}/T_{\parallel}$ . The contribution from  $\Gamma_{RC}$  is important at lower  $\beta_{\parallel}$  and higher  $T_{\perp}/T_{\parallel}$  for the mirror-mode unstable region of parameter space and at lower values of  $T_{\perp}/T_{\parallel}$  for the oblique firehose unstable region. For the stable data, the average value of  $\Gamma_R$  is  $\sim 0$  except for the boundary regions of stable parameter space where either  $T_{\perp}/T_{\parallel} < 0.3$  or  $T_{\perp}/T_{\parallel} > 2$ . This result is consistent for both  $\Gamma_{RI}$  and  $\Gamma_{RC}$ , although we see some variance in the sign of  $\Gamma_{RI}$  at the boundary to the mirror-mode unstable region.

We verify from the probability density functions (not shown here) of  $\Gamma_R$  for each of the

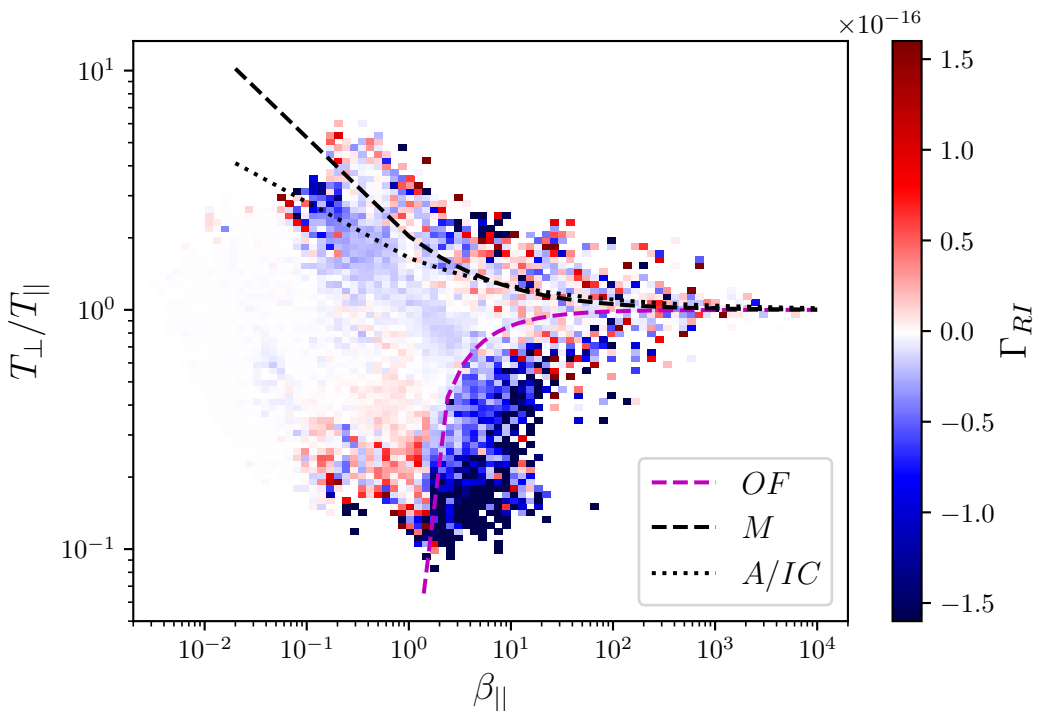


FIGURE 2. Distribution of  $\Gamma_{RI}$  as bin averages in  $T_{\perp}/T_{\parallel}-\beta_{\parallel}$  parameter space. We overplot the instability thresholds for the Oblique Firehose (OF), Alfvén/Ion cyclotron (A/IC), and Mirror-mode (M) instabilities.

stable ( $\Gamma_R^S$ ), oblique firehose unstable ( $\Gamma_R^{OF}$ ), and mirror-mode unstable ( $\Gamma_R^M$ ) regions that the magnitude of the averaged  $\Gamma_R$  is consistently larger in the unstable measurement intervals and that the contrast with the stable region is not simply an averaging effect. We find the mean values as  $\langle \Gamma_R^S \rangle = -3.76 \times 10^{-18} \text{ J cm}^3 \text{ s}^{-1}$ ,  $\langle \Gamma_R^{OF} \rangle = -4.95 \times 10^{-17} \text{ J cm}^3 \text{ s}^{-1}$  and  $\langle \Gamma_R^M \rangle = 3.51 \times 10^{-17} \text{ J cm}^3 \text{ s}^{-1}$ , where  $\langle \cdot \rangle$  represents the average over all measurement intervals in the respective category.

#### 4. Intermittency

In this section, we analyse statistical moments, specifically the third (skewness) and fourth (kurtosis) moments, to measure the intermittency of  $\Gamma_R$ . We compare this result with the skewness and kurtosis of the background magnetic and velocity fields.

Intermittency of magnetic and electric fields and plasma parameters (velocity, density, temperature) in the inertial range has been extensively studied (Tu & Marsch 1995; Marsch & Tu 1997; Sorriso-Valvo *et al.* 1999; Bruno *et al.* 2001). We examine the statistical measures separately for stable and unstable intervals to understand the dynamics of the driving of anisotropy by the turbulent fluctuations. In particular, we investigate how the intermittency (in the sense of ‘burstiness’) of the pressure strain varies across the relevant scales.

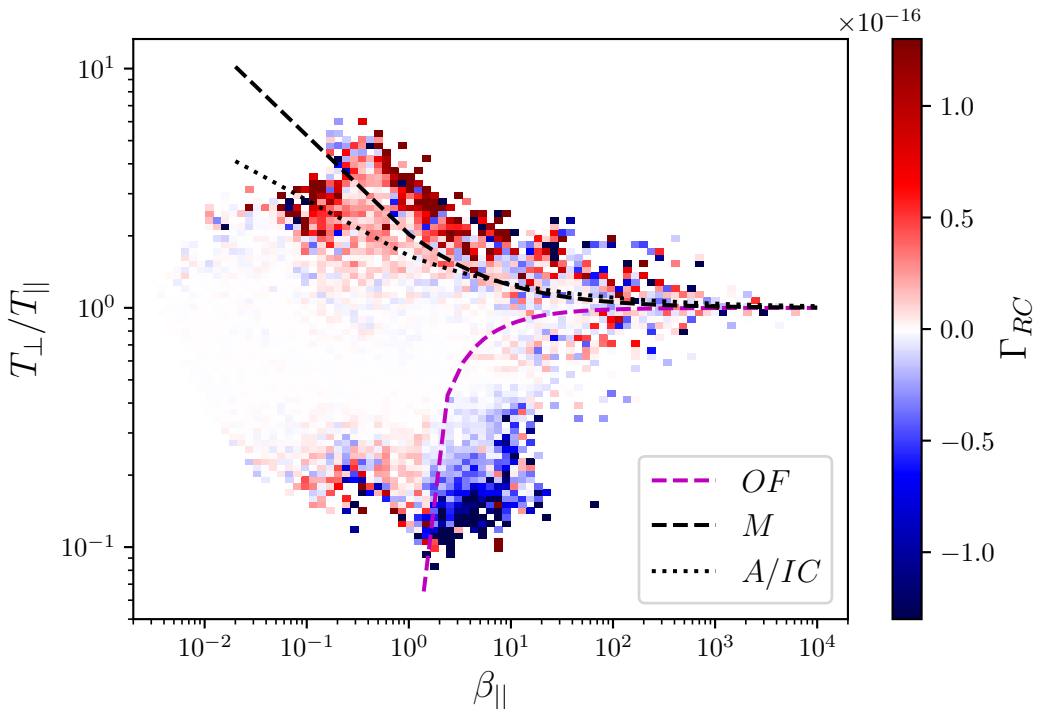


FIGURE 3. Distribution of  $\Gamma_{RC}$  as bin averages in  $T_{\perp}/T_{\parallel}-\beta_{\parallel}$  parameter space. We overplot the instability thresholds for the Oblique Firehose (OF), Alfvén/Ion cyclotron (A/IC), and Mirror-mode (M) instabilities.

#### 4.1. Method: Measuring the Skew and Kurtosis across scales

We use the statistical moments of the quantities  $\mu_i$  to calculate their skewness  $\lambda_i$  and their kurtosis  $\kappa_i$ , where  $\mu_i$  is the moment about the mean. The moments are defined as

$$\lambda_i = \frac{\langle \mu_i^3 \rangle}{\langle \mu_i^2 \rangle^{3/2}}. \quad (4.1)$$

and

$$\kappa_i = \frac{\langle \mu_i^4 \rangle}{\langle \mu_i^2 \rangle^2} \quad (4.2)$$

Using Equations 4.1 and 4.2, we calculate  $\lambda_i$  and  $\kappa_i$  for  $\Gamma_R$ ,  $\mathbf{B}$  and  $\mathbf{V}$ . We calculate  $\lambda_i$  and  $\kappa_i$  for the whole dataset and for each of the stable, oblique firehose unstable, and mirror-mode unstable datasets.

We also calculate  $\lambda_{\Gamma_R}$  and  $\kappa_{\Gamma_R}$  across a range of temporal scales. We do this by creating scale-dependent datasets for  $\Gamma_R$  using Equation (3.2) with  $\tau \in \{8 \text{ s}, 16 \text{ s}, 32 \text{ s}, 64 \text{ s}, 128 \text{ s}, 256 \text{ s}, 512 \text{ s}, 1024 \text{ s}, 2048 \text{ s}\}$ . This results in scale-dependent values of  $\lambda_{\Gamma_R}$  and  $\kappa_{\Gamma_R}$  from the small-scale end of the inertial range up to the correlation-length scale.



	$\kappa_i$	$\kappa_i^S$	$\kappa_i^{OF}$	$\kappa_i^M$	$\lambda_i$	$\lambda_i^S$	$\lambda_i^{OF}$	$\lambda_i^M$
$\Gamma_R$	6.97e4	4.78e3	1.65e4	4.17e3	-134	-4.03	-117	+61.7
$\mathbf{V}$	4.78	4.84	2.69	2.43	+1.05	+1.07	+0.31	+0.602
$\mathbf{B}$	16.0	15.8	3.26	4.43	+2.86	+2.86	+0.389	+0.816

TABLE 2. Skewness  $\lambda_i$  and kurtosis  $\kappa_i$  for  $\Gamma_R$ ,  $\mathbf{V}$ , and  $\mathbf{B}$  across all data, stable intervals, and unstable intervals.

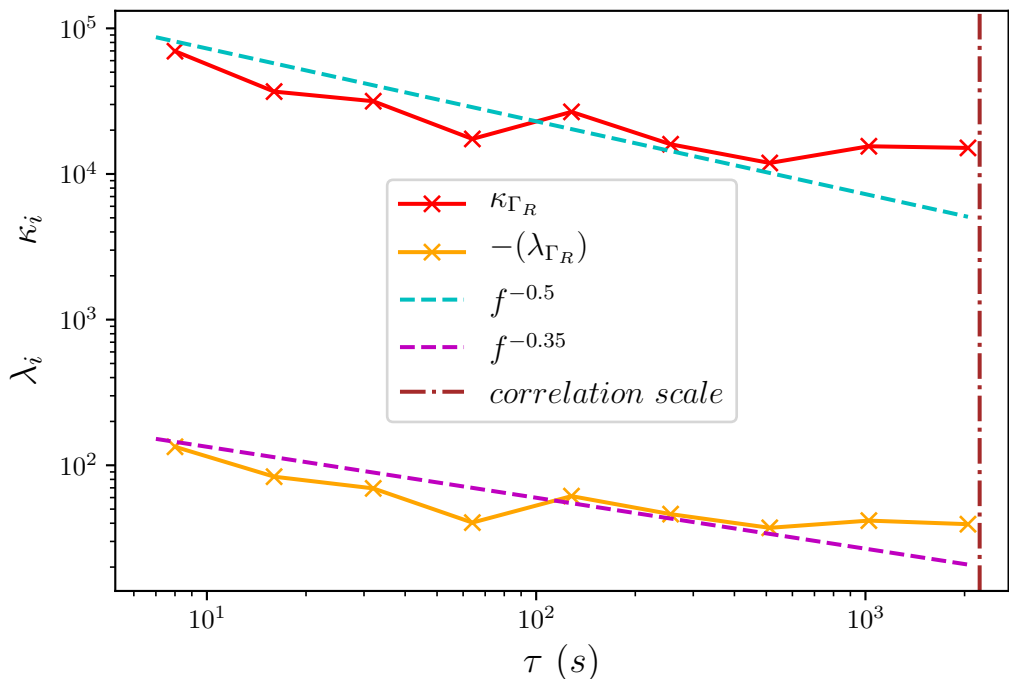


FIGURE 4.  $\lambda_{\Gamma_R}$  and  $\kappa_{\Gamma_R}$  over a range of temporal scales  $\tau$  from 8 s to 2048 s. The cyan and magenta dashed lines represent a power-law scaling of  $-0.5$  and  $-0.35$  respectively. The brown vertical dash-dotted line represents the correlation scale.

#### 4.2. Results: The intermittency of $\Gamma_R$

We show the values obtained for  $\lambda_i$  and  $\kappa_i$  in Table 2. The values of  $\lambda_i$  indicate a symmetric distribution in nearly all cases except for  $\lambda_{\Gamma_R}^{OF}$  which is strongly negative and  $\lambda_{\Gamma_R}^M$  which is strongly positive, while the overall  $\lambda_{\Gamma_R}$  is also strongly negative.

We see that  $\kappa_{\Gamma_R} \gg \kappa_{\mathbf{V}}$  and  $\kappa_{\Gamma_R} \gg \kappa_{\mathbf{B}}$ ; in both cases by 2–3 orders of magnitude. This is expected since  $\Gamma_R$  is built by multiplying intermittent quantities, and its normalised moments will therefore correspond to higher-order moments when compared with  $\mathbf{V}$  and  $\mathbf{B}$ . For the conditioned subsets of  $\Gamma_R$ ,  $\kappa_{\Gamma_R}^{OF} > \kappa_{\Gamma_R}^S \approx \kappa_{\Gamma_R}^M$ .

We calculate  $\lambda_i$  and  $\kappa_i$  for  $\Gamma_{RI}$  and  $\Gamma_{RC}$ .  $\lambda_{\Gamma_{RI}} \approx -104$  is negative while  $\lambda_{\Gamma_{RC}} \approx +46$  is positive.  $\kappa_{\Gamma_{RI}} \approx 5.1e4$  and  $\kappa_{\Gamma_{RC}} \approx 3.05e4$  are consistent with  $\kappa_{\Gamma_R}$ .

Figure 4 shows the scale-dependent values of  $\lambda_{\Gamma_R}$  and  $\kappa_{\Gamma_R}$  as a function of  $\tau$ . Both  $\lambda_{\Gamma_R}$  and  $\kappa_{\Gamma_R}$  show a power-law scaling which is overlaid as indicated. The values for  $\lambda_{\Gamma_R}$

show that the skewness of  $\Gamma_R$  increases with decreasing scale from a local minimum at  $\tau \approx 512$  s. The sign of all values of  $\lambda_{\Gamma_R}$  is negative and has been reversed for visualisation on the logarithmic axis.

The values of  $\kappa_{\Gamma_R}$  indicate that the burstiness of the field increases with decreasing scale, which is the signature of scale-dependent statistics typical of intermittency. Over all  $\tau$  in this figure, the  $\Gamma_R$  field is evidently intermittent and hence ‘bursty’ due to a heavy-tailed distribution of  $\Gamma_R$ . The value of  $\kappa_{\Gamma_R}$  reaches a local minimum at  $\tau \approx 512$  s.

## 5. Discussion

Under the assumptions underlying Equation (3.1) in Section 3, shear and compression create pressure anisotropy (Squire *et al.* 2023), and we interpret our findings as being consistent with that prediction. Relative to the stable data, the absolute values of the bin-averaged  $\Gamma_R$  for the unstable data are significantly elevated, on average by a factor of ten. Our interpretation for this observation is that the presence of data in unstable intervals requires the pressure strain from turbulence-driven shears and compressions to compete with the instabilities that act to restore the plasma towards isotropy. In effect, data can only reside in unstable conditions if the timescale associated with the pressure-strain driving of temperature anisotropy is sufficiently small compared to the relaxation time of the relevant instabilities.

Previous work demonstrates that temperature anisotropy and vorticity are well correlated in hybrid simulations of plasma turbulence (Franci *et al.* 2016). Hybrid-kinetic simulations also show that oblique firehose and mirror-mode instabilities can be driven by a changing magnetic field in a shear flow (Kunz *et al.* 2014). Our results suggest that the turbulent shears in the velocity field create and modulate temperature anisotropy through a purely dynamical process such as that proposed by Del Sarto & Pegoraro (2018) and observed in near-Earth space (Servidio *et al.* 2014; Sorriso-Valvo 2019). In this scenario, the non-compressive turbulent fluctuations result in spatially intermittent velocity shears that modulate the frozen-in magnetic field and drive  $T_{\perp}/T_{\parallel} \neq 1$  with a corresponding change in magnetic field strength (Del Sarto *et al.* 2016; Del Sarto & Pegoraro 2018; Squire *et al.* 2023).

We also see a role for compressive fluctuations in this scenario as seen in Figure 3 where the distribution of  $\Gamma_{RC}$  is similar to the distribution of  $\Gamma_R$ . Figure 3 also shows that the contribution from compressive fluctuations to  $\Gamma_R$  in unstable intervals has the highest absolute average values where  $T_{\perp}/T_{\parallel}$  approaches its maximum (M) or minimum (OF) bounds. In particular, we infer from comparison with Figure 2 that compressive fluctuations are important in driving temperature anisotropy that creates conditions unstable to the mirror-mode instability. This is consistent with previous findings concerning the distribution of magnetic field fluctuations in unstable intervals (Opie *et al.* 2023). We expect the contribution from  $\Gamma_{RC}$  to be less significant overall since compressive fluctuations only account for a minor fraction of the solar wind turbulent energy (Tu & Marsch 1995; Bruno & Carbone 2013; Verscharen *et al.* 2019; Marino & Sorriso-Valvo 2023).

The role of  $\Gamma_R$  in driving mirror-mode unstable conditions is further supported by the skewness of  $\Gamma_R$  and its conditioned subsets where, as set out in Section 4, both  $\lambda_{\Gamma_{RC}}$  and  $\lambda_{\Gamma_R}^M$  are positive while  $\lambda_i$  is negative for the other subsets or close to zero for  $\lambda_{\Gamma_R}^S$ .

In the solar wind, the instabilities once triggered, act on timescales that rapidly reduce the temperature anisotropy (Bandyopadhyay 2022; Opie *et al.* 2022, 2023). The persistence of unstable intervals is, however, observable over extended spatial and temporal scales (Opie *et al.* 2022). Although we cannot fully exclude the possibility that  $\Gamma_R$

reflects the fluctuations created by the instabilities themselves rather than the anisotropy-driving background turbulence, this persistence time-scale argument suggests that the temperature anisotropies are indeed driven by the plasma motions. In addition to the consideration of the magnitude of  $\Gamma_R$ , an analysis of the normalised cross-helicity and the Alfvén ratio shows that there are structural differences in the turbulence in the unstable regions (see Appendix A). This analysis suggests that there is an imbalance relative to the stable data whereby on average the energy in the velocity field is greater than that in the magnetic field for the unstable intervals. A further discussion of these structural differences would be worthwhile in a future study.

We note that our use of the radial rate of strain is distinct from the pressure strain interaction – the so-called Pi-D formalism – analysis that examines the contribution of turbulent fluctuations to the heat flux at ion scales (Yang *et al.* 2017; Bandyopadhyay 2020; Yang 2023). Nonetheless, our formulation goes some way to explaining the relationship between velocity shears and temperature anisotropy noted as an open question by Yang *et al.* (2017).

Similarly, our measure differs from the Partial Variation of Increments (PVI) which is used to locate magnetic (or velocity) field structures in solar-wind turbulence (Greco *et al.* 2008, 2017). The radial rate of strain  $\Gamma_R$  is a dynamical measure that does not involve normalisation by a long-term average and is applied directly to fluctuations in the velocity field. We use  $\Gamma_R$  to identify the creation of temperature anisotropy. We calculate the Pearson correlation coefficients between PVI and  $\Gamma_R$  for our complete dataset and separately for each of the three conditioned subsets defined by stable, oblique firehose unstable, and mirror-mode unstable intervals. We find negligible to no correlation with coefficients that range from  $\approx 0.09$  for the stable data to  $\approx 0.003$  for the whole dataset.

Observations and simulations suggest an important role for turbulent structures in the evolution of plasma conditions in the solar wind (Osman *et al.* 2012; Servidio *et al.* 2014; Franci *et al.* 2015; Greco *et al.* 2017; Sorriso-Valvo *et al.* 2017; Hellinger *et al.* 2019; Qudsi *et al.* 2020). In Section 4, we use statistical analysis to link the role of  $\Gamma_R$  in driving unstable conditions with the skewness and kurtosis of  $\Gamma_R$ ,  $\mathbf{B}$ , and  $\mathbf{V}$ . We apply this analysis to the conditioned subsets denoted as stable, oblique firehose unstable, mirror-mode unstable. The large kurtosis of  $\Gamma_R$  and its subsets show that  $\Gamma_R$  is highly intermittent and exhibits burstiness to a greater degree than either  $\mathbf{B}$  or  $\mathbf{V}$ . We see that  $\kappa_{\Gamma_R}^{OF}$  is considerably greater than either  $\kappa_{\Gamma_R}^M$  or  $\kappa_{\Gamma_R}^S$  which is not the case for the subsets of  $\mathbf{B}$  or  $\mathbf{V}$ .

Coupled with the values for the skewness, we find three distinct subsets of  $\Gamma_R$  with positively and negatively skewed subsets being associated with the oblique firehose and mirror-mode instabilities respectively whilst for the stable data the skewness is nearly zero. The fact that the overall magnitudes of the skewness and kurtosis of  $\Gamma_R$  are greater than those for the individual subsets implies that additional intermittency comes precisely from the alternation of these three distinct regions of stable data, firehose unstable data and mirror-mode unstable data.

The power-law scalings of  $\lambda_{\Gamma_R}$  and  $\kappa_{\Gamma_R}$  shown in Figure 4 follow an exponent that is compatible with standard intermittency in the solar-wind magnetic field (Sorriso-Valvo *et al.* 1999). This correspondence is not unexpected since  $\Gamma_R$  is built using various intermittent quantities. However, it implies that the greater magnitudes of  $\lambda_{\Gamma_R}$  and  $\kappa_{\Gamma_R}$  relative to those of  $\mathbf{B}$  and  $\mathbf{V}$  are not scale-dependent. We should therefore expect to see the regions of stable, oblique firehose unstable, and mirror-mode unstable data characterised by distinct subsets of  $\Gamma_R$  across scales in the inertial range of solar-wind turbulence.

While it has long been known that the turbulence in the solar wind is intermittent

and multifractal (Paladin & Vulpiani 1987; Burlaga 1991; Tu & Marsch 1995; Frisch & Kolmogorov 1995), the analysis of our statistically robust, large dataset quantifies these characteristics in a novel way, allowing us to treat separately stable and unstable intervals in the data. Calculation from observations of all the quantities in this study requires the use of incremental gradients, and we benefit from Solar Orbiter’s in-situ instrument suite that provides continuous high-resolution datasets over significant timescales to enable this. The scientific impacts of the efficiency and high resolution of these instruments are by now well documented (Rouillard 2020; D’Amicis 2021; Louarn 2021; Opie *et al.* 2022; Zouganelis *et al.* 2022). Nevertheless, our measures are restricted by the use of single-spacecraft data, which confines all analyses in this work to the radial sampling direction. In our view, the most promising route to extend this work lies in the use of high-quality three-dimensional data from a multi-spacecraft mission. This extension would allow the estimation of all relevant three-dimensional gradients rather than sampling along the radial direction via Taylor’s hypothesis only. It would also be useful to extend the range of radial distances from the Sun over which these analyses are made using the perihelia data from Solar Orbiter and Parker Solar Probe.

Previous work shows how unstable intervals are statistically spatially and temporally distributed (Opie *et al.* 2022) and that unstable intervals are ergodicity-breaking and therefore statistically disjoint with respect to the stable regime (Opie *et al.* 2023). Our current findings support and extend these previous results and describe more fully the impact of turbulence on kinetic instabilities in the solar wind, and in particular quantify the role of  $\Gamma_R$  in driving unstable conditions.

## 6. Conclusions

In this work, we show that solar-wind intervals with parameters above the thresholds for temperature-anisotropy-driven instabilities are on average characterised by high absolute values of  $\Gamma_R$  which is a measure of the extent to which bulk motions in the plasma drive temperature anisotropy. We attribute this observational result to the proposition that strong velocity shears drive temperature anisotropies in the turbulent solar wind through the shearing of the frozen-in magnetic field with a double-adiabatic impact on the particle distributions.

The radial rate of strain  $\Gamma_R$  is highly intermittent with a distribution that exhibits greater levels of kurtosis relative to those of  $\mathbf{B}$  and  $\mathbf{V}$  which is not unexpected given the contribution of increments of both  $\mathbf{B}$  and  $\mathbf{V}$  in Equation 3.2. Nonetheless, we attribute this observational result to the burstiness of velocity shears in the solar wind with a significant occurrence rate of extreme values leading to a heavy-tailed distribution of  $\Gamma_R$ . The conditioned subsets of  $\Gamma_R$  that relate to stable, oblique firehose unstable, and mirror-mode unstable intervals comprise distributions that are characteristically asymmetric (or symmetric in the case of stable data). The alternation of these distinct subsets contributes to the intermittency of  $\Gamma_R$ . We attribute this observational result to the inhomogeneity that distinguishes each of the three regions of  $T_\perp/T_\parallel - \beta_\parallel$  parameter space represented by the subsets and that are both statistically and physically disjoint. Our observational measures – skewness and kurtosis – exhibit power-law scalings with an exponent that is consistent with the known intermittency in solar-wind turbulence.

Our study opens several areas of extended interest that deserve further exploration. For turbulence studies, our results emphasise the importance of the velocity field for the temperature anisotropy (and potentially other kinetic properties) of the plasma. We suggest that an analysis of the Local Energy Transfer (LET) measure derived from the Politano–Pouquet scaling law (Politano & Pouquet 1998; Sorriso-Valvo *et al.* 2018b)

revised to account for pressure-anisotropic magnetohydrodynamic turbulence (Simon & Sahraoui 2022) would be a useful extension of the current study. In addition, the role of  $\Gamma_R$  in solar-wind turbulence could be further investigated in the simulation domain, ideally building on the existing work that shows how fluctuations in the velocity field are related to anisotropy (Franci *et al.* 2015, 2016, 2018; Hellinger *et al.* 2019).

Our work highlights new science opportunities for multi-spacecraft missions such as HelioSwarm (Klein 2023) and Plasma Observatory (Retinò 2022), which will provide a means of measuring fully three-dimensional rates of strain and intermittency. These data will enable a more precise unpicking of the contributions of non-compressive and compressive fluctuations as well as intermittency to the creation and modulation of temperature anisotropy. A mission like HelioSwarm or Plasma Observatory with their complements of fields and plasma instrumentation has thus the potential to create breakthroughs in our understanding of the interplay between turbulence and kinetic instabilities in space plasmas. In particular, our results suggest that accurate and high-resolution measurements of the velocity field will be of fundamental importance to this task.

Our investigation of Solar Orbiter observations reveals a consistent picture of where and under what conditions kinetic instabilities act at the relevant scales in the turbulent solar wind. Unstable intervals are located in regions of strong velocity shear embedded in rapidly changing structures in the intermittent turbulence of the velocity field. The velocity shear and its associated impact on the frozen-in magnetic field drives and modulates the temperature anisotropy necessary to create the unstable conditions. The plasma can only remain above the instability thresholds for as long as the shears are sufficient to overcome the relaxation through the instabilities. This process takes place predominantly at the shear layers of highly intermittent structures whose distribution is strongly non-Gaussian. Accordingly, the presence of instabilities is not evenly distributed either spatially or temporally in the solar wind plasma.

## Appendix A. Alfvénicity in the solar wind

For this analysis of the Alfvénicity, we consider the fluctuations on the scale of 2 min, which is at the small-scale end of the inertial range and captures the relevant scales for the persistence of unstable intervals (Opie *et al.* 2022). We define

$$\delta\mathbf{b} = \mathbf{B} - \|\mathbf{B}_0\| \quad (\text{A } 1)$$

and

$$\delta\mathbf{v} = \mathbf{V} - \|\mathbf{V}_0\|, \quad (\text{A } 2)$$

where  $\|\cdot\|$  denotes the time average taken over a 2-minute interval centred on the time of the measurement of  $\delta\mathbf{b}$  and  $\delta\mathbf{v}$ .

We define the normalised cross-helicity as

$$\sigma_c = \frac{2(\delta\mathbf{v} \cdot \delta\mathbf{b})}{(|\delta\mathbf{v}|^2 + |\delta\mathbf{b}|^2)} \quad (\text{A } 3)$$

and the Alfvén ratio as

$$R_A = \frac{|\delta\mathbf{v}|^2}{|\delta\mathbf{b}|^2}. \quad (\text{A } 4)$$

With these definitions, we create point-wise datasets for  $\sigma_c$  and  $R_A$  that allow us to investigate the correlations of the magnetic field and velocity field fluctuations at the scale of 2 min.

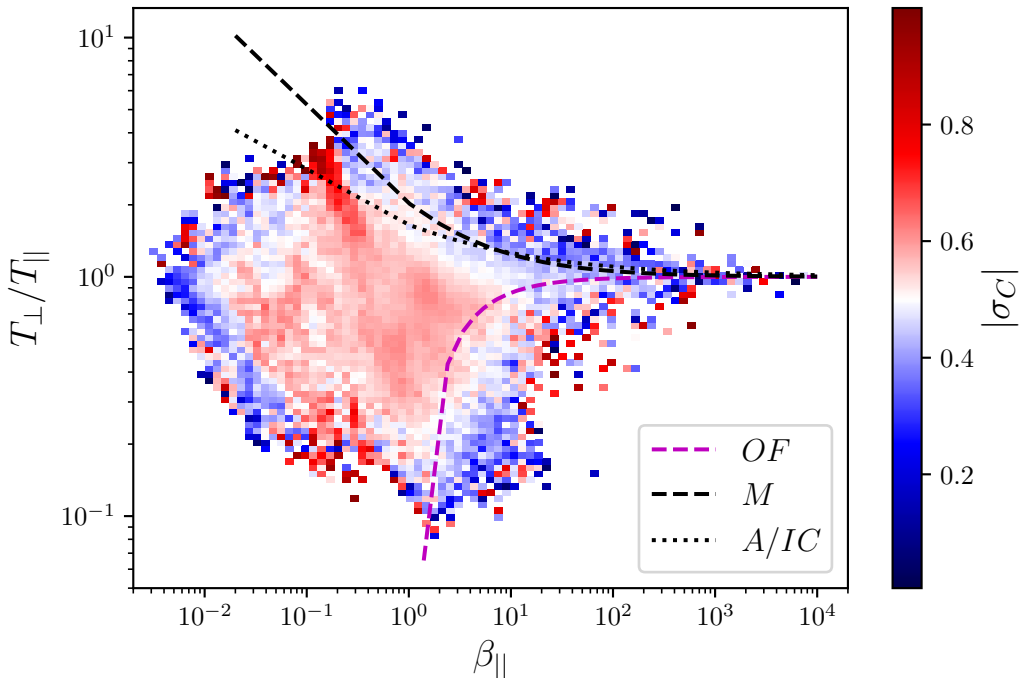


FIGURE 5. Distribution of  $|\sigma_c|$  as bin averages in  $T_\perp/T_\parallel$ - $\beta_\parallel$  parameter space. We overplot the instability thresholds for Oblique Firehose (OF), Alfvén/Ion cyclotron (A/IC), and Mirror-mode (M) instabilities.

We show  $|\sigma_c|$  and  $R_A$  as bin-averaged distributions in  $T_\perp/T_\parallel$ - $\beta_\parallel$  parameter space for our whole dataset in Figures 5 and 6.

On average, normalised cross-helicity in the solar wind is higher near the core of the stable dataset in this parameter space and lower in the unstable intervals and at the low- $\beta_\parallel$  boundary of the stable data. The distribution of the bin-averaged Alfvén ratio shows that  $|\delta\mathbf{v}|^2 \gg |\delta\mathbf{b}|^2$  in the unstable regions of parameter space when  $T_\perp/T_\parallel \leq 0.6$  or  $T_\perp/T_\parallel \geq 1.6$ .

We see that  $\sigma_c$  is significantly lower on average in the unstable intervals relative to the stable data, suggesting an imbalance between the velocity and magnetic field fluctuations in the unstable regions of the  $T_\perp/T_\parallel$ - $\beta_\parallel$  parameter space. This is consistent with the hypothesis of a restriction on the amplitude of Alfvénic fluctuations in the limit of the oblique firehose instability (Squire *et al.* 2016, 2017) and suggests a similar mechanism may apply in the limit of the mirror-mode instability. The distribution of bin-averaged  $R_A$  demonstrates that in the unstable intervals greater temperature anisotropy is associated with the dominance of energy in the velocity field over energy in the magnetic field so that  $R_A \gg 1$ .

## Declaration of Interests

Declaration of Interests. The authors report no conflict of interest.

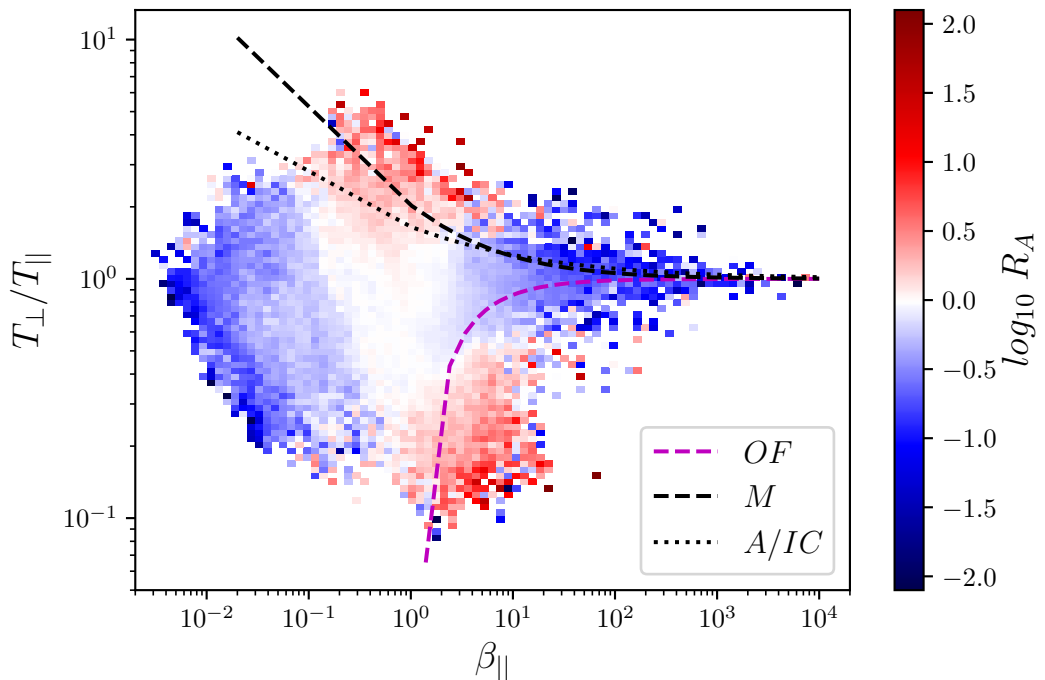


FIGURE 6. Distribution of  $R_A$  plotted as bin averages in  $T_{\perp}/T_{\parallel}-\beta_{\parallel}$  parameter space with instability thresholds shown for Oblique Firehose (OF), Alfvén/Ion cyclotron (A/IC) and Mirror-mode (M) instabilities.

## Acknowledgements

S.O. is supported by NERC grant NE/S007229/1. D.V. and C.J.O. are supported by STFC Consolidated Grant ST/W001004/1. CHKC is supported by UKRI Future Leaders Fellowship MR/W007657/1 and STFC Consolidated Grants ST/T00018X/1 and ST/X000974/1. P.A.I. is supported by NSF grant AGS2005982. L.F. is supported by the Royal Society University Research Fellowship No. URF/R1/231710 and by UKRI/STFC grant ST/W001071/1. This research was discussed at the International Space Science Institute (ISSI) in Bern, through ISSI International Team project #563 (Ion Kinetic Instabilities in the Solar Wind in Light of Parker Solar Probe and Solar Orbiter Observations) led by L. Ofman and L. Jian. Solar Orbiter is a space mission of international collaboration between ESA and NASA, operated by ESA. Solar Orbiter Solar Wind Analyser (SWA) data are derived from scientific sensors which have been designed and created, and are operated under funding provided in numerous contracts from the UK Space Agency (UKSA), STFC, the Agenzia Spaziale Italiana (ASI), the Centre National d'Études Spatiales (CNES), the Centre National de la Recherche Scientifique (CNRS), the Czech contribution to the ESA PRODEX programme, and NASA. Solar Orbiter SWA work at UCL/MSSL is currently funded under STFC grants ST/T001356/1 and ST/S000240/1. The Solar Orbiter magnetometer was funded by UKSA grant ST/T001062/1.

## REFERENCES

- ALEXANDROVA, O., CHEN, C. H. K., SORRISO-VALVO, L., HORBURY, T. S. & BALE, S. D. 2013 Solar Wind Turbulence and the Role of Ion Instabilities. *Space Science Reviews* **178** (2-4), 101–139.
- ARZAMASSKIY, LEV, KUNZ, MATTHEW W., SQUIRE, JONATHAN, QUATAERT, ELIOT & SCHEKOCIHIN, ALEXANDER A. 2023 Kinetic Turbulence in Collisionless High-Beta Plasmas. *Physical Review X* **13** (2), 021014.
- BALE, S. D., KASPER, J. C., HOWES, G. G., QUATAERT, E., SALEM, C. & SUNDKVIST, D. 2009 Magnetic Fluctuation Power Near Proton Temperature Anisotropy Instability Thresholds in the Solar Wind. *Physical Review Letters* **103** (21), 211101.
- BANDYOPADHYAY, RIDDHI, ET AL. 2020 Statistics of Kinetic Dissipation in the Earth's Magnetosheath: MMS Observations. *Physical Review Letters* **124** (25), 255101.
- BANDYOPADHYAY, RIDDHI, ET AL. 2022 Interplay of turbulence and proton-microinstability growth in space plasmas. *Physics of Plasmas* **29** (10), 102107.
- BRUNO, ROBERTO & CARBONE, VINCENZO 2013 The Solar Wind as a Turbulence Laboratory. *Living Reviews in Solar Physics* **10**.
- BRUNO, R., CARBONE, V., VELTRI, P., PIETROPAOLO, E. & BAVASSANO, B. 2001 Identifying intermittency events in the solar wind. *Planetary and Space Science* **49** (12), 1201–1210.
- BURLAGA, L.F. 1991 Intermittent turbulence in the solar wind. *Journal of Geophysical Research: Space Physics* **96** (A4), 5847–5851.
- CARBONE, VINCENZO, BRUNO, ROBERTO & VELTRI, PIERLUIGI 1996 Evidences for extended self-similarity in hydromagnetic turbulence. *Geophysical Research Letters* **23** (2), 121–124.
- CARBONE, VINCENZO, VELTRI, PIERLUIGI & BRUNO, ROBERTO 1995 Experimental Evidence for Differences in the Extended Self-Similarity Scaling Laws between Fluid and Magnetohydrodynamic Turbulent Flows. *Physical Review Letters* **75** (17), 3110–3113.
- CHANDRAN, BENJAMIN D. G., LI, BO, ROGERS, BARRETT N., QUATAERT, ELIOT & GERMASCHEWSKI, KAI 2010 Perpendicular Ion Heating by Low-frequency Alfvén-wave Turbulence in the Solar Wind. *The Astrophysical Journal* **720** (1), 503–515.
- CHEN, C. H. K. 2016 Recent progress in astrophysical plasma turbulence from solar wind observations. *Journal of Plasma Physics* **82** (6).
- CHEN, C. H. K., MATTEINI, L., SCHEKOCIHIN, A. A., STEVENS, M. L., SALEM, C. S., MARUCA, B. A., KUNZ, M. W. & BALE, S. D. 2016 Multi-Species Measurements of the Firehose and Mirror Instability Thresholds in the Solar Wind. *The Astrophysical Journal* **825** (2), L26.
- CHEW, G.F., LOW, F.E. & GOLDBERGER, M.L. 1956 The Boltzmann equation and the one-fluid hydromagnetic equations in the absence of particle collisions. *Proceedings of the Royal Society of London. Series A. Mathematical and Physical Sciences* **236** (1204), 112–118.
- CHO, JUNGYEON & VISHNIAC, ETHAN T. 2000 The Anisotropy of Magnetohydrodynamic Alfvénic Turbulence. *The Astrophysical Journal* **539** (1), 273.
- COBURN, JESSE T., CHEN, CHRISTOPHER H. K. & SQUIRE, JONATHAN 2022 A measurement of the effective mean free path of solar wind protons. *Journal of Plasma Physics* **88** (5), 175880502.
- COLEMAN, JR., PAUL J. 1968 Turbulence, Viscosity, and Dissipation in the Solar-Wind Plasma. *The Astrophysical Journal* **153**, 371.
- CRANMER, STEVEN R., MATTHAEUS, WILLIAM H., BREECH, BENJAMIN A. & KASPER, JUSTIN C. 2009 Empirical Constraints on Proton and Electron Heating in the Fast Solar Wind. *The Astrophysical Journal* **702** (2), 1604.
- DEL SARTO, DANIELE & PEGORARO, FRANCESCO 2018 Shear-induced pressure anisotropization and correlation with fluid vorticity in a low collisionality plasma. *Monthly Notices of the Royal Astronomical Society* **475** (1), 181–192.
- DEL SARTO, D., PEGORARO, F. & CALIFANO, F. 2016 Pressure anisotropy and small spatial scales induced by velocity shear. *Physical Review E* **93** (5), 053203.
- D'AMICIS, R., ET AL. 2021 First Solar Orbiter observation of the Alfvénic slow wind and identification of its solar source. *Astronomy & Astrophysics* **656**, A21.
- FRANCI, LUCA, HELLINGER, PETR, MATTEINI, LORENZO, VERDINI, ANDREA & LANDI, SIMONE 2016 Two-dimensional hybrid simulations of kinetic plasma turbulence: Current and vorticity vs proton temperature. *AIP Conference Proceedings* **1720** (1), 040003.
- FRANCI, LUCA, LANDI, SIMONE, MATTEINI, LORENZO, VERDINI, ANDREA & HELLINGER,



- PETR 2015 High-resolution Hybrid Simulations of Kinetic Plasma Turbulence at Proton Scales. *The Astrophysical Journal* **812** (1), 21.
- FRANCI, LUCA, LANDI, SIMONE, VERDINI, ANDREA, MATTEINI, LORENZO & HELLINGER, PETR 2018 Solar Wind Turbulent Cascade from MHD to Sub-ion Scales: Large-size 3D Hybrid Particle-in-cell Simulations. *The Astrophysical Journal* **853** (1), 26.
- FRISCH, U. & KOLMOGOROV, A. N. 1995 *Turbulence: the legacy of A.N. Kolmogorov*. Cambridge, [Eng.]; New York: Cambridge University Press.
- FRISCH, URIEL, SULEM, PIERRE-LOUIS & NELKIN, MARK 1978 A simple dynamical model of intermittent fully developed turbulence. *Journal of Fluid Mechanics* **87** (4), 719–736.
- GARY, S. PETER 1976 Proton temperature anisotropy instabilities in the solar wind. *Journal of Geophysical Research (1896-1977)* **81** (7), 1241–1246.
- GARY, S. PETER 1993 *Theory of space plasma microinstabilities. Cambridge atmospheric and space science series 7*. Cambridge: Cambridge University Press.
- GARY, S. PETER 2015 Short-wavelength plasma turbulence and temperature anisotropy instabilities: recent computational progress. *Philosophical Transactions of the Royal Society A: Mathematical, Physical and Engineering Sciences* **373** (2041), 20140149.
- GRECO, A., CHUYCHAI, P., MATTHAEUS, W. H., SERVIDIO, S. & DMITRUK, P. 2008 Intermittent MHD structures and classical discontinuities. *Geophysical Research Letters* **35** (19).
- GRECO, A., MATTHAEUS, W. H., PERRI, S., OSMAN, K. T., SERVIDIO, S., WAN, M. & DMITRUK, P. 2017 Partial Variance of Increments Method in Solar Wind Observations and Plasma Simulations. *Space Science Reviews* **214** (1), 1.
- HELLINGER, PETR, LANDI, SIMONE, MATTEINI, LORENZO, VERDINI, ANDREA & FRANCI, LUCA 2017 Mirror Instability in the Turbulent Solar Wind. *The Astrophysical Journal* **838** (2), 158.
- HELLINGER, PETR, MATTEINI, LORENZO, LANDI, SIMONE, FRANCI, LUCA, VERDINI, ANDREA & PAPINI, EMANUELE 2019 Turbulence versus Fire-hose Instabilities: 3D Hybrid Expanding Box Simulations. *The Astrophysical Journal* **883** (2), 178.
- HELLINGER, PETR, MATTEINI, LORENZO, ŠTVERÁK, ŠTĚPÁN, TRÁVNÍČEK, PAVEL M. & MARSCH, ECKART 2011 Heating and cooling of protons in the fast solar wind between 0.3 and 1 AU: Helios revisited. *Journal of Geophysical Research: Space Physics* **116** (A9).
- HELLINGER, PETR, TRÁVNÍČEK, PAVEL, KASPER, JUSTIN C. & LAZARUS, ALAN J. 2006 Solar wind proton temperature anisotropy: Linear theory and WIND/SWE observations. *Geophysical Research Letters* **33** (9).
- HELLINGER, PETR & TRÁVNÍČEK, PAVEL M. 2008 Oblique proton fire hose instability in the expanding solar wind: Hybrid simulations. *Journal of Geophysical Research: Space Physics* **113** (A10).
- HELLINGER, PETR, TRÁVNÍČEK, PAVEL M., ŠTVERÁK, ŠTĚPÁN, MATTEINI, LORENZO & VELLI, MARCO 2013 Proton thermal energetics in the solar wind: Helios reloaded. *Journal of Geophysical Research: Space Physics* **118** (4), 1351–1365.
- HNAT, B., CHAPMAN, S. C., KIYANI, K., ROWLANDS, G. & WATKINS, N. W. 2007 On the fractal nature of the magnetic field energy density in the solar wind. *Geophysical Research Letters* **34** (15).
- HORBURY, T. S., ET AL. 2020 The Solar Orbiter magnetometer. *Astronomy & Astrophysics* **642**, A9.
- HORBURY, T. S., WICKS, R. T. & CHEN, C. H. K. 2012 Anisotropy in Space Plasma Turbulence: Solar Wind Observations. *Space Science Reviews* **172** (1-4), 325–342.
- HOWES, G. G. 2015 A dynamical model of plasma turbulence in the solar wind. *Philosophical Transactions of the Royal Society A: Mathematical, Physical and Engineering Sciences* **373** (2041), 20140145.
- ISENBERG, PHILIP A., MARUCA, BENNETT A. & KASPER, JUSTIN C. 2013 Self-Consistent Ion Cyclotron Anisotropy-Beta Relation for Solar Wind Protons. *The Astrophysical Journal* **773** (2), 164.
- KASPER, JUSTIN C., LAZARUS, ALAN J. & GARY, S. PETER 2002 Wind/SWE observations of firehose constraint on solar wind proton temperature anisotropy. *Geophysical Research Letters* **29** (17), 20–1–20–4.
- KIYANI, K., CHAPMAN, S. C. & HNAT, B. 2006 Extracting the scaling exponents of a self-

- affine, non-Gaussian process from a finite-length time series. *Physical Review E* **74** (5), 051122.
- KIYANI, KHUROM H., OSMAN, KAREEM T. & CHAPMAN, SANDRA C. 2015 Dissipation and heating in solar wind turbulence: from the macro to the micro and back again. *Philosophical Transactions of the Royal Society A: Mathematical, Physical and Engineering Sciences* **373** (2041), 20140155.
- KLEIN, KRISTOPHER G., ET AL. 2023 HelioSwarm: A Multipoint, Multiscale Mission to Characterize Turbulence. *Space Science Reviews* **219** (8), 74.
- KOLMOGOROV, ANDREY NIKOLAEVICH 1941 Dissipation of Energy in Locally Isotropic Turbulence. *Akademiia Nauk SSSR Doklady* **32**, 16.
- KULSRUD, R. M. 1984 *MHD description of plasma*. North-Holland Publishing Company, conference Name: Basic Plasma Physics: Selected Chapters, Handbook of Plasma Physics, Volume 1 Pages: 115 ADS Bibcode: 1984bpp..conf..115K.
- KUNZ, MATTHEW W., SCHEKOCIHIN, ALEXANDER A. & STONE, JAMES M. 2014 Firehose and Mirror Instabilities in a Collisionless Shearing Plasma. *Physical Review Letters* **112** (20), 205003.
- LOUARN, P., ET AL. 2021 Multiscale views of an Alfvénic slow solar wind: 3D velocity distribution functions observed by the Proton-Alpha Sensor of Solar Orbiter. *Astronomy & Astrophysics* **656**, A36.
- MARINO, RAFFAELE & SORRISO-VALVO, LUCA 2023 Scaling laws for the energy transfer in space plasma turbulence. *Physics Reports* **1006**, 1–144.
- MARKOVSKII, S. A. & VASQUEZ, BERNARD J. 2022 The Effect of Solar Wind Turbulence on Parallel and Oblique Firehose Instabilities. *The Astrophysical Journal* **924** (2), 111.
- MARSCH, E., MÜHLHÄUSER, K.-H., SCHWENN, R., ROSENBAUER, H., PILIPP, W. & NEUBAUER, F. M. 1982 Solar wind protons: Three-dimensional velocity distributions and derived plasma parameters measured between 0.3 and 1 AU. *Journal of Geophysical Research: Space Physics* **87** (A1), 52–72.
- MARSCH, E. & TU, C.-Y. 1997 Intermittency, non-Gaussian statistics and fractal scaling of MHD fluctuations in the solar wind. *Nonlinear Processes in Geophysics* **4** (2), 101–124, publisher: Copernicus GmbH.
- MARUCA, B. A., KASPER, J. C. & BALE, S. D. 2011 What Are the Relative Roles of Heating and Cooling in Generating Solar Wind Temperature Anisotropies? *Physical Review Letters* **107** (20), 201101.
- MATTEINI, LORENZO, HELLINGER, PETR, LANDI, SIMONE, TRÁVNÍČEK, PAVEL M. & VELLI, MARCO 2012 Ion Kinetics in the Solar Wind: Coupling Global Expansion to Local Microphysics. *Space Science Reviews* **172** (1-4), 373–396.
- MATTEINI, LORENZO, LANDI, SIMONE, HELLINGER, PETR, PANTELLINI, FILIPPO, MAKSIMOVIC, MILAN, VELLI, MARCO, GOLDSTEIN, BRUCE E. & MARSCH, ECKART 2007 Evolution of the solar wind proton temperature anisotropy from 0.3 to 2.5 AU. *Geophysical Research Letters* **34** (20), L20105.
- MATTHAEUS, W. H., WAN, MINPING, SERVIDIO, S., GRECO, A., OSMAN, K. T., OUGHTON, S. & DMITRUK, P. 2015 Intermittency, nonlinear dynamics and dissipation in the solar wind and astrophysical plasmas. *Philosophical Transactions of the Royal Society A: Mathematical, Physical and Engineering Sciences* **373** (2041), 20140154.
- MÖSTL, CHRISTIAN, WEISS, ANDREAS J., BAILEY, RACHEL L., REISS, MARTIN A., AMERSTORFER, TANJA, HINTERREITER, JÜRGEN, BAUER, MAIKE, MCINTOSH, SCOTT W., LUGAZ, NOÉ & STANSBY, DAVID 2020 Prediction of the In Situ Coronal Mass Ejection Rate for Solar Cycle 25: Implications for Parker Solar Probe In Situ Observations. *The Astrophysical Journal* **903** (2), 92.
- MÖSTL, C., ET AL. 2017 Modeling observations of solar coronal mass ejections with heliospheric imagers verified with the Heliophysics System Observatory. *Space Weather* **15** (7), 955–970.
- OPIE, SIMON, VERSCHAREN, DANIEL, CHEN, CHRISTOPHER H. K., OWEN, CHRISTOPHER J. & ISENBERG, PHILIP A. 2022 Conditions for Proton Temperature Anisotropy to Drive Instabilities in the Solar Wind. *The Astrophysical Journal* **941** (2), 176.
- OPIE, SIMON, VERSCHAREN, DANIEL, CHEN, CHRISTOPHER H. K., OWEN, CHRISTOPHER J. & ISENBERG, PHILIP A. 2023 The effect of variations in the magnetic field direction from turbulence on kinetic-scale instabilities. *Astronomy & Astrophysics* **672**, L4.

- OSMAN, K. T., MATTHAEUS, W. H., HNAT, B. & CHAPMAN, S. C. 2012 Kinetic Signatures and Intermittent Turbulence in the Solar Wind Plasma. *Physical Review Letters* **108** (26), 261103.
- OSMAN, K. T., MATTHAEUS, W. H., KIYANI, K. H., HNAT, B. & CHAPMAN, S. C. 2013 Proton Kinetic Effects and Turbulent Energy Cascade Rate in the Solar Wind. *Physical Review Letters* **111** (20), 201101.
- OUGHTON, S., MATTHAEUS, W. H., WAN, M. & OSMAN, K. T. 2015 Anisotropy in solar wind plasma turbulence. *Philosophical Transactions of the Royal Society A: Mathematical, Physical and Engineering Sciences* **373** (2041), 20140152.
- OWEN, C. J., ET AL. 2020 The Solar Orbiter Solar Wind Analyser (SWA) suite. *Astronomy & Astrophysics* **642**, A16.
- PALADIN, GIOVANNI & VULPIANI, ANGELO 1987 Anomalous scaling laws in multifractal objects. *Physics Reports* **156** (4), 147–225.
- PARASHAR, T. N., SHAY, M. A., CASSAK, P. A. & MATTHAEUS, W. H. 2009 Kinetic dissipation and anisotropic heating in a turbulent collisionless plasma. *Physics of Plasmas* **16** (3), 032310.
- POLITANO, H. & POUQUET, A. 1998 von Kármán–Howarth equation for magnetohydrodynamics and its consequences on third-order longitudinal structure and correlation functions. *Physical Review E* **57** (1), R21–R24.
- QUDSI, R. A., MARUCA, B. A., MATTHAEUS, W. H., PARASHAR, T. N., BANDYOPADHYAY, RIDDHI, CHHIBER, R., CHASAPIS, A., GOLDSTEIN, MELVYN L., BALE, S. D., BONNELL, J. W., WIT, T. DUDOK DE, GOETZ, K., HARVEY, P. R., MACDOWALL, R. J., MALASPINA, D., PULUPA, M., KASPER, J. C., KORRECK, K. E., CASE, A. W., STEVENS, M., WHITTLESEY, P., LARSON, D., LIVI, R., VELLI, M. & RAOUAFI, N. 2020 Observations of Heating along Intermittent Structures in the Inner Heliosphere from  $\mathcal{PSP}$  Data. *The Astrophysical Journal Supplement Series* **246** (2), 46, publisher: American Astronomical Society.
- RETINÒ, ALESSANDRO, ET AL. 2022 Particle energization in space plasmas: towards a multi-point, multi-scale plasma observatory. *Experimental Astronomy* **54** (2), 427–471.
- ROUILLARD, A. P., ET AL. 2020 Models and data analysis tools for the Solar Orbiter mission. *Astronomy & Astrophysics* **642**, A2.
- SCHEKOCHIHIN, ALEXANDER A. 2022 MHD turbulence: a biased review. *Journal of Plasma Physics* **88** (5), 155880501.
- SCHEKOCHIHIN, A. A., COWLEY, S. C., DORLAND, W., HAMMETT, G. W., HOWES, G. G., QUATAERT, E. & TATSUNO, T. 2009 Astrophysical gyrokinetics: kinetic and fluid turbulent cascades in magnetized weakly collisional plasmas. *The Astrophysical Journal Supplement Series* **182** (1), 310–377.
- SERVIDIO, S., OSMAN, K. T., VALENTINI, F., PERRONE, D., CALIFANO, F., CHAPMAN, S., MATTHAEUS, W. H. & VELTRI, P. 2014 Proton Kinetic Effects in Vlasov and Solar Wind Turbulence. *The Astrophysical Journal* **781** (2), L27.
- SIMON, P. & SAHRAOUI, F. 2022 Exact law for compressible pressure-anisotropic magnetohydrodynamic turbulence: Toward linking energy cascade and instabilities. *Physical Review E* **105** (5), 055111.
- SORRISO-VALVO, LUCA, ET AL. 2019 Turbulence-Driven Ion Beams in the Magnetospheric Kelvin-Helmholtz Instability. *Physical Review Letters* **122** (3), 035102.
- SORRISO-VALVO, LUCA, CARBONE, FRANCESCO, LEONARDIS, ERSILIA, CHEN, CHRISTOPHER H. K., ŠAFRÁNKOVÁ, JANA & NĚMEČEK, ZDENEK 2017 Multifractal analysis of high resolution solar wind proton density measurements. *Advances in Space Research* **59** (6), 1642–1651.
- SORRISO-VALVO, LUCA, CARBONE, FRANCESCO, PERRI, SILVIA, GRECO, ANTONELLA, MARINO, RAFFAELE & BRUNO, ROBERTO 2018a On the Statistical Properties of Turbulent Energy Transfer Rate in the Inner Heliosphere. *Solar Physics* **293** (1), 10.
- SORRISO-VALVO, LUCA, CARBONE, VINCENZO, VELTRI, PIERLUIGI, CONSOLINI, GIUSEPPE & BRUNO, ROBERTO 1999 Intermittency in the solar wind turbulence through probability distribution functions of fluctuations. *Geophysical Research Letters* **26** (13), 1801–1804.
- SORRISO-VALVO, LUCA, PERRONE, DENISE, PEZZI, ORESTE, VALENTINI, FRANCESCO, SERVIDIO, SERGIO, ZOUGANELIS, IOANNIS & VELTRI, PIERLUIGI 2018b Local energy

- transfer rate and kinetic processes: the fate of turbulent energy in two-dimensional hybrid Vlasov–Maxwell numerical simulations. *Journal of Plasma Physics* **84** (2), 725840201.
- SQUIRE, J., KUNZ, M. W., ARZAMASSKIY, L., JOHNSTON, Z., QUATAERT, E. & SCHEKOCHIHIN, A. A. 2023 Pressure anisotropy and viscous heating in weakly collisional plasma turbulence. *Journal of Plasma Physics* **89** (4), 905890417.
- SQUIRE, J., QUATAERT, E. & SCHEKOCHIHIN, A. A. 2016 A Stringent Limit on the Amplitude of Alfvénic Perturbations in High-Beta Low-Collisionality Plasmas. *The Astrophysical Journal Letters* **830** (2), L25.
- SQUIRE, J., SCHEKOCHIHIN, A. A. & QUATAERT, E. 2017 Amplitude limits and nonlinear damping of shear-Alfvén waves in high-beta low-collisionality plasmas. *New Journal of Physics* **19** (5), 055005.
- TAYLOR, G. I. 1938 The Spectrum of Turbulence. *Proceedings of the Royal Society A: Mathematical, Physical and Engineering Sciences* **164** (919), 476–490.
- TU, C-Y & MARSCH, ECKART 1995 MHD structures, waves and turbulence in the solar wind: Observations and theories. *Space Science Reviews* **73** (1-2), 1–210.
- VERSCHAREN, DANIEL, CHANDRAN, BENJAMIN D. G., KLEIN, KRISTOPHER G. & QUATAERT, ELIOT 2016 Collisionless isotropization of the solar-wind protons by compressive fluctuations and plasma instabilities. *The Astrophysical Journal* **831** (2), 128.
- VERSCHAREN, DANIEL, KLEIN, KRISTOPHER G. & MARUCA, BENNETT A. 2019 The multi-scale nature of the solar wind. *Living Reviews in Solar Physics* **16** (1).
- WICKS, R. T., HORBURY, T. S., CHEN, C. H. K. & SCHEKOCHIHIN, A. A. 2011 Anisotropy of Imbalanced Alfvénic Turbulence in Fast Solar Wind. *Physical Review Letters* **106** (4), 045001.
- YANG, YAN, ET AL. 2023 Quantifying the Anisotropy of Proton and Electron Heating in Turbulent Plasmas. *The Astrophysical Journal* **944** (2), 148.
- YANG, YAN, MATTHAEUS, WILLIAM H., PARASHAR, TULASI N., HAGGERTY, COLBY C., ROYTERSHEYN, VADIM, DAUGHTON, WILLIAM, WAN, MINPING, SHI, YIPENG & CHEN, SHIYI 2017 Energy transfer, pressure tensor, and heating of kinetic plasma. *Physics of Plasmas* **24** (7), 072306.
- ZOUGANELIS, YANNIS, LARIO, DAVID, VERSCHAREN, DANIEL & ZHUKOV, ANDREI 2022 Solar orbiter: Up-close view of the sun and inner heliosphere in situ. In *Fall Meeting 2022*. AGU.